Effective Electrochemical n-Type Doping of ZnO Thin films for Optoelectronic Window Applications

Paula Cembrero-Coca,[a] M. Mollar,[a] K. C. Singh,[b] and B. Marí[a,z]

[a]*Departament de Física Aplicada -IDF, Universitat Politècnica de València, Camí de Vera s/n, 46022 València, Spain*
[b]*Department of Chemistry, Maharshi Dayanand University, Rohtak, 124001 Haryana, India*

An effective n-type doping of ZnO thin films electrochemically synthetized was achieved by varying the chloride ion concentration in the starting electrolyte. The ratio between chloride and zinc cations was varied between 0 and 2 while the zinc concentration in the solution was kept constant. When the concentration of chloride in the bath increases an effective n-type doping of ZnO films takes place. n-type doping is evidenced by the rise of donors concentration, obtained from Mott-Schottky measurements, as well as from the blueshift observed in the optical gap owing to the Burstein-Moss effect.

ZnO with low resistivity, high transmittance down to the UV spectral range, and good chemical stability under strong reducing environments is a promising transparent conductive oxide (TCO) to be used as transparent electrode for photovoltaic solar cells and electrodes on flat panel displays.[1] This role is presently reserved to conventional TCOs like FTO (Fluorine-doped tin oxide) and ITO (Indium tin oxide). Nevertheless, one of the advantages of ZnO is that can be electrochemically deposited on practically any conductive substrate. Unintentionally doped ZnO thin films are always n-type due to the presence of native donors.[2] However, for some applications a greater conductivity is required and then n-type doping has to be boosted by increasing the concentration of shallow donors. In ZnO, additional n-type doping can be attained by using group III metal elements such as Al, Ga or In, which substitute Zn. The conductivity increase depends upon the nature and amount of the ions incorporated. Up to now, metal elements like Al,[3,4] Ga,[5,6] Ba,[7] Sc,[7] Sn[8] and In[8] have been widely used for this purpose. On the other hand, elements of 1B group (Cu, Ag, Au) act as acceptors when substituting Zn. Recently, p-type behavior has been reported in Cu-doped ZnO films.[9]

Further, the substitution of ZnO lattice anions can also result in an increase of the conductivity even though this option has been less explored. Substituting O by VII group elements, such as F or Cl, also results in an effective n-type doping. There are a few studies where fluor[10,11] or chlorine[12–15] replace oxygen. It is always found the doping with extrinsic ions increases conductivity and decreases transparency of films. However, the use of non-metal dopants in substitution to O was suggested as a better way to achieve high carrier concentration and mobility while keeping good transparency, due to the weaker perturbation of the ZnO conduction band expected in this configuration.[12,16]

Until now, most of the research on the deposition methods has mainly been focused on vapor-phase techniques.[17] A common characteristic of these kinds of techniques is the high temperature. Temperatures around 900–1100°C are the most frequently used in vapor−liquid−solid processes,[18,19] while lower temperatures of 400−500°C are used in free-catalyst and more sophisticated techniques such as metal−organic chemical vapor deposition.[20] Electrochemical deposition of ZnO nanowire arrays, from the reduction of molecular oxygen in aqueous solutions, is a convenient low-temperature (<100°C) alternative.[21,22] Aside from the fact that this technique is well-suited for large-scale production processes, electrodeposited ZnO nanowire arrays have already shown great potentiality in nanostructured solar cells,[23] ultraviolet (UV) electroluminescent hybrid light emitting diodes,[24] and UV nanolasers.[25] Several species such as nitrate ions,[26,27] molecular oxygen,[28,29] hydrogen peroxide[30] have been used as oxygen precursors and ZnCl$_2$, Zn(ClO$_4$)$_2$, Zn(NO$_3$)$_2$, Zn(SO$_4$) and Zn(CH$_3$COO)$_2$, etc. are used as Zn^{2+} precursors[31,32] for the electrodeposition of ZnO. We have used the mixtures of ZnCl$_2$ and Zn(ClO$_4$)$_2$ solutions in Dimethylsulfoxide (DMSO) saturated with molecular O$_2$ for the electrodeposition of ZnO films at 80 degree. The extent of doping of chloride is found to depends upon the molar ratio of the [Cl$^-$]/[Zn^{2+}] ions in the solution.

In this paper a systematic study of the electrodeposition of n-type Cl$^-$ doped ZnO thin films is presented and the influence of the chloride concentration introduced in the electrolyte on the optoelectronic properties of the deposited films is described. X-ray diffraction (XRD), Scanning Electron Microscope (SEM), optical properties and electrochemical impedance spectroscopy measurements (Mott-Schottky) have been used to assess the shallow donors concentration into ZnO:Cl films. The increase of the free carrier concentration results in a partial filling of the conduction band and then in a blueshift of the apparent bandgap explained by the Burstein-Moss effect.

Experimental

ZnO films were electrodeposited from DMSO solutions containing always a constant concentration (25 mM) of Zn^{2+}. Zn^{2+} cations were obtained by dissolving two different types of salts, chlorides and perchlorates. ZnCl$_2$ (Merck, reagent grade) and Zn(ClO$_4$)$_2$ *6H$_2$O (Aldrich, reagent grade) were used to prepare solutions in such a way that the ratio between chloride and zinc ions was varied while the zinc concentration was kept constant, as shown in Table I. 0.1 M KClO$_4$ (Sigma–Aldrich, reagent grade) was used as a supporting electrolyte. The bath solution was saturated by oxygen gas bubbling through the electrolyte.

The electrodeposition process of ZnO was carried out in a three-electrode electrochemical cell. Glass slides of about 1×2 cm coated with F-doped SnO$_2$ (FTO) and sheet resistance of ~10 $\Omega \cdot$ square were used as working electrode. Previously, the substrate was cleaned with soap water, rinsed with acetone and finally cleaned ultrasonically in ethanol. Pt counter electrode and Ag/AgCl (KCl 3M) reference electrode (+210 mV vs Normal Hydrogen Electrode, NHE) were used. AutoLab PGStat 302N potentio/galvanostat was used for maintaining a constant potential (V = −0.9 V) during the electrodeposition process. The temperature of the bath was kept constant at $80 \pm 0.5°$C. ZnO films with thicknesses of about 700 and 1400 nm were obtained for deposited charges of −1C and −2C, respectively.

Characterization.— The compositions of the films were studied using a Scanning Electron Microscope (SEM, JEOL-JSM6300) operating at 20 kV, coupled to an Energy Dispersive Spectroscopy (EDS) detector.

The structural properties of these films were characterized by X-ray diffraction (XRD, Rigaku Ultima IV diffractometer) in Bragg-Brentano configuration using a CuK$_\alpha$ radiation ($\lambda = 1.5418$ Å). The diffraction pattern was scanned by steps of 0.02 (2θ) between 25° and 70°.

[z]E-mail: bmari@fis.upv.es

Table I. Content of dissolved salts (zinc chloride, zinc perchlorate and potassium perchlorate) and [Cl⁻]/[Zn] ratio in the starting bath.

[ZnCl$_2$] mM	[Zn(ClO$_4$)$_2$] mM	[KClO$_4$] mM	[Cl$^-$]/[Zn^{2+}]
25.0	0.0	100	2.00
19.0	6.0	100	1.52
12.5	12.5	100	1.00
6.0	19.0	100	0.48
0.0	25.0	100	0.00

Optical properties were monitored by a HR4000 Ocean Optics spectrometer with a combined halogen-deuterium lamp DT-MINI-2 for the UV-VIS range.

Electrochemical impedance spectroscopy (EIS) measurements were carried out with AutoLab PGSTAT 302N potentio/galvanostat equipped with a FRA module. Dissolution of 0.1 M of KClO$_4$ was used as electrolyte. Each measurement was registered by applying a 10 mV AC sinusoidal signal with a frequency of 10 kHz. The potential scan in the range -0.75 V to 0.2 was carried out. All measurements were done at room temperature.

Results and Discussion

X-ray diffraction and SEM.— Because the use of different ratios of Cl$^-$ and ClO$^-_4$ in deposition solutions can result in the formation of different insoluble species, X-ray diffraction was used to investigate the presence of some spurious crystalline phases in the obtained films.
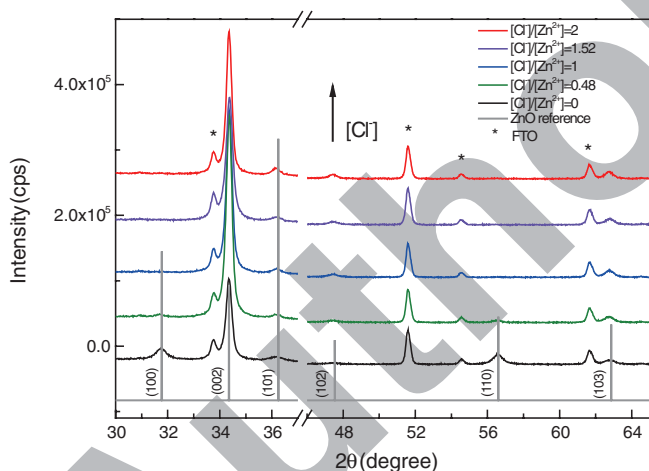

Figure 1. XRD patterns of ZnO thin films grown in electrolytes containing different chloride concentrations.
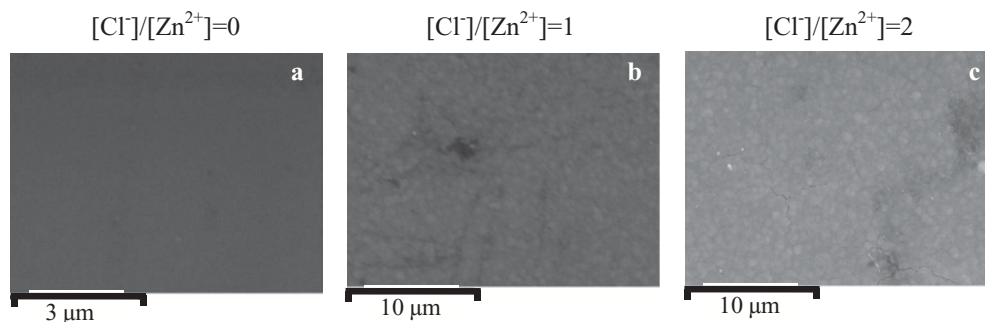
Figure 1 summarizes the X-ray diffraction (XRD) patterns of samples electrodeposited in different ratios of [Cl$^-$]/[Zn^{2+}] solutions for films with two coulombs of deposited charge. All diffraction peaks can be indexed by considering only FTO phase from the TCO substrates and the ZnO wurzite phase. Irrespective of the deposition solution, no spurious phases were detected by XRD. Consequently, the changes of the nature of zinc precursor do not influence the deposition of ZnO wurzite phase.

Under the current deposition conditions ZnO:Cl films are mainly oriented in the (002) direction, which is parallel to the c axis perpendicular to the substrate plane. However, the variation of [Cl$^-$] concentration induces some changes in the intensity of all diffraction peaks. The trend is the higher the [Cl$^-$] concentration in the bath the lower the intensity of peaks with null z component, i.e. (100) and (110) and the higher the intensity of peaks containing z component, i.e. (002), (101), (102) and (103). Therefore it can be concluded that the presence of [Cl$^-$] favors the growth in the direction perpendicular to the substrate while the [ClO$^-_4$] ions promote the growth along the substrate surface. According to this result smoother and more continuous ZnO films are expected to be deposited from baths containing higher contents of perchlorate [ClO$^-_4$] ions.

A similar conclusion can be inferred from SEM observations (Figure 2a, 2b, 2c). Films obtained for all [Cl$^-$]/[Zn^{2+}] ratios present a dense morphology. However, the increase of the chloride amount in the bath results in a slightly variation in the roughness of the films surface. Samples with null chloride concentration (Figure 2a) exhibits a perfectly smooth surface where no signs of roughness can be observed while in films obtained from baths containing chlorides (Figure 2b and 2c) some grains can be observed. This result indicate that the rise of the roughness is related with the growth perpendicular to the substrate plane and is in good agreement with the dependence of the main crystallographic growth direction for ZnO:Cl films with the [Cl$^-$] or [ClO$^-_4$] contents as previously deduced from XRD experiments. Several examples of electrochemical ZnO growth perpendicular to the surface with columnar or tube-shaped morphologies from baths containing only chlorides can be found in the literature.[31,33]

The EDX analysis reveals that the doping of Cl atomic concentration ranges from 0.7% to 5% for a pure perchlorate electrolyte to pure chloride electrolyte. The detection of chlorine in the material, even if no ZnCl$_2$ is added to the electrolyte, shows that perchlorate ions can also act as a source of chloride. But this effect is much weaker than that of adding chloride ions in the bath. The atomic concentration of chlorine in the film increases as a function of chloride concentration in the bath. The samples were cleaned with deionized water directly after the growth in order to eliminate eventual chloride salt traces on film surfaces. So the EDX measurements are expected to show the incorporation of chlorine atoms into the ZnO bulk. Table II displays the relative Cl concentration in the electrodeposited film as a function of the [Cl$^-$]/[Zn^{2+}] ratio of the electrolyte. Although the quantitative assessment of the Cl concentration is difficult with this technique we are able to evidence the linearity between Cl atoms in the film and Cl$^-$ concentration ions present in the starting electrolyte.

$[Cl^-]/[Zn^{2+}]=0$ $[Cl^-]/[Zn^{2+}]=1$ $[Cl^-]/[Zn^{2+}]=2$

Figure 2. SEM images of ZnO films deposited with various [Cl$^-$]/[Zn^{2+}] ratios: (**a**) 0, (**b**) 1 and (**c**) 2.

Table II. Relative concentration of Cl atoms in thin film obtained from EDX measurements.

ZnCl$_2$/ (ZnCl$_2$+Zn(ClO$_4$)$_2$)	[Cl$^-$]/[Zn^{2+}]	Cl (at%)
1.00	2.00	5.0
0.75	1.52	4.5
0.50	1.00	3.6
0.25	0.48	3.2
0.00	0.00	0.7

Electrical properties.— It has been demonstrated by Rousset et al.[15] that in ZnO lattice Cl substitution replaces the O, thus introducing an extrinsic donor level that can play a role on the electrical properties of the samples. According to that higher n-type level of doping of ZnO films can be achieved by increasing the content of Cl into the ZnO lattice.

Mott-Schottky measurements have been carried out in order to evaluate the impact of electrolyte nature on the electrical properties of the deposited material. This method is based on the Schottky barrier formation between the semiconductor material and the electrolyte.[34–36] If the electrolyte is concentrated enough, the voltage drop due to the inverse polarization and the Schottky barrier are completely distributed in the semiconductor material. It causes the creation of a depletion zone that can be characterized by a capacitance measurement. If the system obeys Mott-Schottky behavior, the evolution of $1/C^2$ is a linear function of the applied potential. The sign and the value of its slope is representative of the doping type and of the carrier concentration (N), respectively. This latter can be determined from the slope of this curve, using the equation:

$$\frac{1}{C^2} = \left(\frac{2}{e\varepsilon_0\varepsilon_r N_D A^2}\right)\left(V - V_{FB} - \frac{kT}{e}\right) \qquad [1]$$

Where C is the capacitance of the space charge region of the film at potential V, V_{FB} is the flatband potential, N_D is the donor concentration, A is the delimited area in contact with the electrolyte, the assumption of a perfectly smooth surface is made, ε_0 is the permittivity of the free space, and ε_r the relative dielectric constant taken as the typical value for bulk ZnO ($\varepsilon_r = 8.0$). The Mott-Schottky plots obtained on the films deposited in different ratios of [Cl$^-$]/[Zn^{2+}] electrolytes are shown in Figure 3.

Figure 3. Mott-Schottky plots for ZnO:Cl thin films with different amount of Cl.

Table III. Results for the calculation of donor densities (column b), estimation of flatbands potentials (column c) and optical bangaps (column d) for ZnO:Cl thin films obtained from electrolytes with different [Cl$^-$]/[Zn^{2+}] ratios (column a). All potentials are referred to Ag/AgCl. Results obtained for bare FTO have also been included.

a) [Cl$^-$]/[Zn^{2+}]	b) N$_d$ (cm^{-3})	c) Flat Band Potencial (V)	d) Eg (eV)
2.00	8.06$10^{19}$	−0.47	3.442
1.52	6.21$10^{19}$	−0.42	3.423
1.00	5.16$10^{19}$	−0.38	3.409
0.48	3.34$10^{19}$	−0.38	3.386
0.00	1.89$10^{19}$	−0.31	3.372
FTO	4.24$10^{20}$	−1.37	

Mott-Schottky plots are related to Mott-Schottky behavior for a small linear potential region between −0.35 and −0.15 V. In the region between −0.35 and 0.25 V, the overall capacitance decreased (increase in $1/C^2$) with increasing film thickness. This is the mark of a n-type semiconductor behavior when the applied potential is shifted to cathodic values. The non-linear behavior of plots from −0.35 V to 0.25 V may be a due to the some assumptions made during the derivation of Mott-Schottky equation are severe. As can be seen from SEM pictures of grown films that there are small grains over the compact films, those cause the non-uniform potential gradients and varying space charge region dimensions through the thickness of the collection of grains within the film.

Table III shows the calculations for donor density N$_d$ and flatband potentials V$_{FB}$ for ZnO:Cl films electrodeposited from electrolytes containing different concentrations of isolated Cl$^-$ ions. The trend is the higher the concentration of Cl$^-$ ions in the electrolyte the higher the donor concentration (N$_d$) in the films, which again is an evidence of the doping effect of Cl in electrodeposited ZnO films. A lowest value of N$_d$ = 1.89 × 10^{19} cm^{-3} is attained for ZnO films synthetized from electrolytes with null concentration of Cl$^-$ ions. When the Cl$^-$ concentration doubles the Zn^{2+} concentration the N$_d$ increases to 8.06 × 10^{19} cm^{-3}. For comparison purposes the donor density for bare FTO has been also calculated. It is well known that, irrespective of the deposition method, unintentionally doped ZnO is always n-type due to the existence of intrinsic defects that act as donors and unavoidably produce n-type doping[2]. In the case of electrodeposited ZnO films this effect is even more important than in other vacuum methods. Subsequent annealing of electrodeposited ZnO thin films always results in a reduction of donor defects concentration and therefore lowers the conductivity of films.

In order to check the changes in the conductivity of ZnO:Cl layers we have measured their sheet resistance by using a four points probe. We found that the sheet resistance varies from 9.7 Ω · square for FTO to 5.4 Ω · square for the most doped ZnO:Cl sample. Even if this is an approximate method for obtaining the sheet resistance because there are two conductive layers and it is not possible to know accurately the contribution of each layer, the measures can always be compared among them.[32]

The flatband potential is shifted to more cathodic values when the chlorine concentration is increased in the electrolyte and this phenomenon is also related to the evolution of the free carrier concentration in the material. The flatband potential becomes more negative as the doping level increases and this fact can be explained as a shift of the Fermi level in the semiconductor, approaching the conduction band as the doping level increases. The increase in the free electron concentration results in a higher surface barrier in the semiconductor-electrolyte interface and then in a larger flatband potential.

In order to better show the linearity of the doping with Cl$^-$ concentration in the electrolyte, N$_d$ values calculated from Mott-Schottky plots are displayed as a function of the [Cl$^-$]/[Zn^{2+}] ratio in the bath Figure 4. The calculated donor concentration exhibits a linear depen-

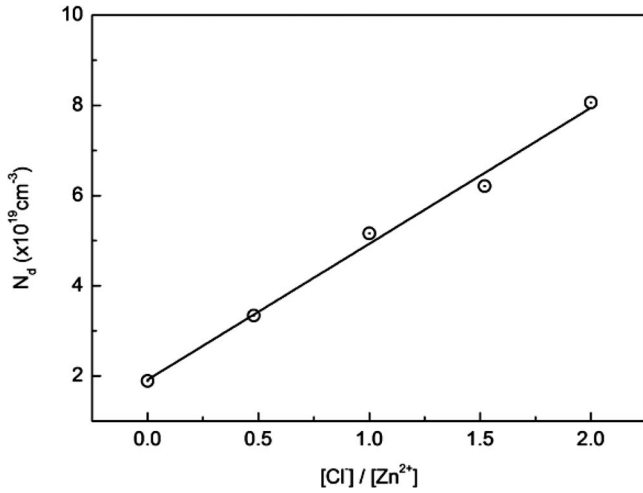**Figure 4.** Donor concentration versus $[Cl^-]/[Zn^{2+}]$ ratio.

Figure 6. Variation of $(\alpha h\upsilon)^2$ as a function of $h\upsilon$.

dence with the amount of Cl^- and the trend is the higher the concentration of isolated Cl^- ions in the electrolyte the higher the donor concentration (N_d). This is a clear evidence of the n-type doping character of Cl atoms in ZnO. The carrier concentration is minimum when the material is synthesized in the pure perchlorate electrolyte (1.89×10^{19} cm^{-3}). The carrier concentration increases more that four times when the films are grown in 100% chloride solution.

Optical properties.— The achievement of high transparency in the visible to near infra-red spectral range is the second important property, besides high conductivity, for the use of ZnO:Cl films as transparent conductors. The visible transmission spectra for ZnO:Cl films with different amount of chloride doping are presented in Figure 5. The transmission is nearly 60% for the films grown in electrolytes without Cl^- ions and nearly 80% transmission is achieved for the films deposited in presence of chloride ions. Higher doping of Cl^- in film leads to higher transmittance.

The optical bandgap energy (Eg) is an intrinsic property of the semiconductor and estimated from optical absorption measurement. The optical transmittance spectra for the thin films recorded over wavelength range 350–700 nm at room temperature. The optical absorption data are analyzed using the following classical relation:

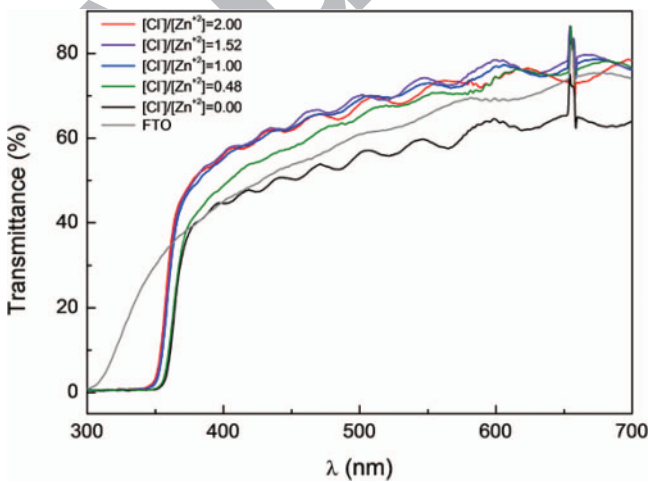$$x = \frac{x_0(h\upsilon - E_g)^n}{h\upsilon} \qquad [2]$$
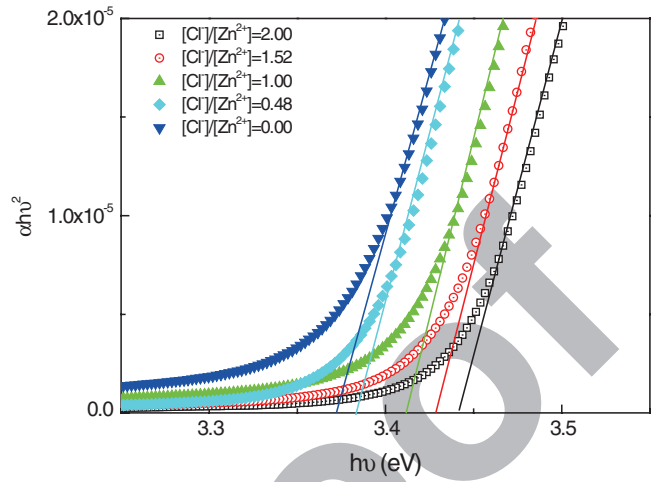

Figure 5. Transmittance curves for ZnO:Cl thin films.

where, Eg is the separation between bottom of the conduction band and top of the valence band, h is the photon energy and n is order. Value of n depends on the probability of transition; it takes values as 1/2, 3/2, 2 and 3 for direct allowed, direct forbidden, indirect allowed and indirect forbidden transitions, respectively. Thus, if plot of $(\alpha h\upsilon)^2$ versus $(h\upsilon)$ is linear the transition is direct allowed. Extrapolation of the straight-line portion to zero absorption coefficient ($\alpha = 0$), leads to estimation of Eg value (Table III, column d). Figure 6 shows variation of $(\alpha h\upsilon)^2$ as a function of photon energy $h\upsilon$.

With increasing Cl^- content, the absorption edge shifted slightly toward lower wavelength region, which means higher bandgaps. The shift of optical bandgap is related to the Burstein-Moss (BM) effect[37] and provides a direct evidence of the doping effect of chloride in ZnO:Cl films.

The Burstein-Moss effect is attributed to the occupation of the conduction band from the electrons coming from the valence band. BM effect shifts the optical absorption edge giving a higher effective bandgap as a result of the longer distance between unoccupied states of the conduction band and the top of the valence band.

The effective optical gap (E_g) can be calculated as the sum of the optical gap for the intrinsic material (E_{g0}) and the increment of the gap due to the BM effect (ΔE_{BM}).

$$E_g = E_{g0} + \Delta E_{BM} \qquad [3]$$

The BM model in n-type semiconductor with parabolic band is given by the equation:[38]

$$\Delta E_{BM} = \frac{h^2}{8\pi^2 m^*}(3\pi^2 n)^{2/3} \qquad [4]$$

Where h is Planck's constant, m^* is the effective mass of the electron and n is the electron free carrier concentration.

Figure 7 shows the experimental values obtained by extrapolation of $(\alpha h\upsilon)^2$ versus $h\upsilon$ (dots) as well as the theoretical values obtained for the bangap of ZnO as a function of the free electron concentration according to equations 3 and 4. Solid blue and red lines are the theoretical bandgap energies for two different effective electron mass found in the literature ($m^* = 0.24 \cdot m_e$[39] and $m^* = 0.35 \cdot m_e$[40]) and for a value of the optical bandgap for the intrinsic material, E_{g0} = 3.263 eV. The experimental points fall inside the theoretical curves for both values of effective electron masses but the slope is lower than expected. In this plot the abscissa is the free electron concentration, n, while the experimental points calculated from Mott-Schottky plots provide the donor concentration, N_D. The free electron concentration depends on both donor and acceptor concentration, N_D and N_A,
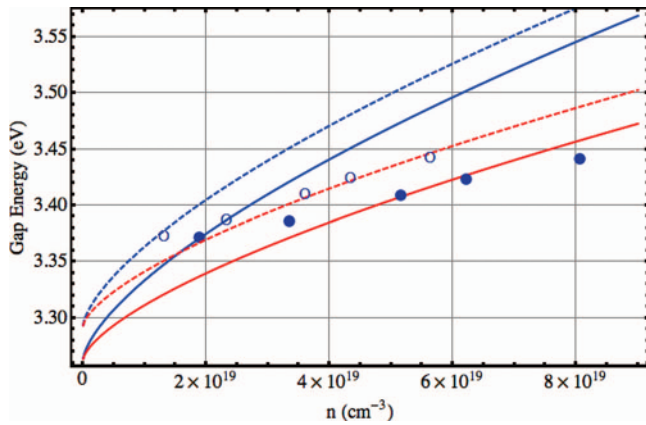
$$n = N_D - N_A \qquad [5]$$

Figure 7. Theoretical calculations of Eg for ZnO as a function of electron concentration (n) for different values of effective electron mass in ZnO. Blue m* = 0.24·me. Red m* = 0.35·me. Solid lines: E_{g0} = 3.263 eV, dashed lines: E_{g0} = 3.293 eV. Experimental values were obtained by extrapolation of $(\alpha h\upsilon)^2$ versus $h\upsilon$. Solid dots: = 0, empty dots: = 0.3.

So, if we define the compensation ratio as the ration between acceptors and donors;

$$\beta = \frac{N_A}{N_D} \qquad [6]$$

the free electron concentration can be written as:

$$n = (1 - \beta) \times N_D \qquad [7]$$

The effect of donor-acceptor compensation has also been displayed in Figure 7. Empty circles represent the free electron concentration obtained from the donor concentration provided by Mott-Schottky by supposing a compensation ratio of 30% (eq. 7). Dashed blue and red lines are the theoretical bandgap energies for the effective electron mass used before and for an intrinsic optical bandgap, E_{g0} = 3.293 eV. After taking into account the donor-acceptor compensation the experimental values fit better to theoretical curves. The consequence of donor-acceptor compensation is to lower the free electron concentration and therefore the occupation of the conduction band. As a result a slightly higher bandgap for the intrinsic material is required to fit the data.

Conclusion

This paper presents a systematic study dealing with the electrodeposition of dense ZnO layers doped with chlorine for transparent conductive oxide applications. The effect of perchlorate electrolyte and the addition of chloride ions in the bath on the morphology, the structure, the carrier concentration and the optical properties of the ZnO layers have been investigated. Compact films with high transmission in the visible wavelengths range and containing high carrier density (up to 9 × 10^19 cm^−3) have been obtained. Compositional analysis, optical and Mott-Schottky measurements allowed demonstrating that n-type doping is extrinsic and achieved by incorporation of chlorine in ZnO lattice. As a result a bandgap shift to higher energies is observed owing to the Burstein-Moss effect.

Electrochemical deposition in electrolytes containing chlorides and DMSO appears to be an attractive way for synthetizing ZnO layers with very high transparency and good control of the conductivity. Due to their low cost synthesis route and good performance, electrodeposited ZnO:Cl layers are well suited to be used in optoelectronic window applications.

References

1. A. Guillén-Santiago, M. de la, L. Olvera, A. Maldonado, R. Asomoza, and D. R. Acosta, *Phys. Stat. Sol. (a).*, **201**, 952 (2004).
2. Fumiyasu Oba, Minseok Choi, Atsushi Togo, and Isao Tanaka, *Sci. Technolo. Adv. Mater.*, **12**, 034302 (2011).
3. Byeong-Yun Oh, Min-Chang Jeong, Woong Lee, and Jae-Min Myoung, *J. Cryst. Growth.*, **274**(3–4), 453 (2005).
4. A. El Manouni, F. J. Manjón, M. Mollar, B. Marí, R. Gómez, M. C. López, and J. R. Ramos-Barrado, *Superlattices and Microstructures*, **39**, 185 (2006).
5. Hiroyuki Kato, Michihiro Sano, Kazuhiro Miyamoto, and Takafumi Yao, *J. Cryst. Growth.*, **237–239**(1), 538 (2002).
6. J. D. Ye, S. L. Gu, S. M. Zhu, S. M. Liu, Y. D. Zheng, R. Zhang, and Y. Shi, *Appl. Phys. Lett.*, **86**, 192111 (2005).
7. Yasunori Morinaga, Keijiro Sakuragi, Norifumi Fujimura, and Taichiro Ito, *J. Cryst. Growth.*, **174**(1–4), 691 (1997).
8. L. Castañeda, A. García-Valenzuela, E. P. Zironi, J. Cañetas-Ortega, M. Terrones, and A. Maldonado, *Thin Solid Films*, **503**, 212 (2006).
9. B. Marí, M. Sahal, M. Mollar, M. F. Cerqueira, and A. Samantilleke, *J. Solid State Electrochem.*, **16**, 2261 (2012).
10. Jianhua Hu and Roy G. Gordon, *Solar Cells*, **30**(1–4), 437 (1991).
11. H. Y. Xu, Y. C. Liu, R. Mu, C. L. Shao, Y. M. Lu, D. z. Shen, and X. W. Fan, *Appl. Phys. Lett.*, **86**, 123107 (2005).
12. J. B. Cui, Y. C. Soo, T. P. Chen, and U. J. Gibson, *J. Phys. Chem. C*, **112**(12), 4475 (2008).
13. T. Tchelidze, E. Chikoidze, O. Gorochov, and P. Galtier, *Thin Solid Films*, **515**(24), 8744 (2007).
14. E. Chikoidze, M. Nolan, M. Modreanu, V. Sallet, and P. Galtier, *Thin Solid Films*, **516**(22), 8146 (2008).
15. J. Rousset, E. Saucedo, and D. Lincot, *Chem. Mater.*, **21**(3), 534 (2009).
16. R. Gordon, *MRS Bull.*, **25**, 52 (2002).
17. Gyu-Chul. Yi, Chunrui Wang, and Won Il Park, *Semicond. Sci. Technol.*, **20**, S22 (2005).
18. M. H. Huang, Y. Wu, H. Feick, N. Tran, E. Weber, and P. Yang, *Adv. Mater.*, **13**(2), 113 (2001).
19. Xudong Wang, Christopher J. Summers, and Zhong Lin Wang, *Nano Letters*, **4**(3), 423 (2004).
20. W. I. Park, D. H Kim, and S. W. Jung, *Appl. Phys. Lett.*, **80**, 423 (2002). Q1
21. M. Davidová, D. Nachtigallová, R. Bulánek, and P. Nachtigall, *J. Phys. Chem. B*, **107**(10), 2327 (2003).
22. O. Bludský, P. Nachtigall, P. Cicmanec, P. Knotek, and R. Bulánek., *Catalysis Today.*, **100**(3–4), 385 (2005).
23. C. Lévy-Clément, R. Tena-Zaera, M. A. Ryan, A. Katty, and G. Hodes, *Adv. Mater.*, **17**(12), 1512 (2005).
24. R. Könenkamp, R. C. Word, and M. Godinez, *Nano Lett.*, **5**(10), 2005 (2005).
25. B. F. Mentzen and G. Bergeret, *J. Phys. Chem. C*, **111**(34), 12512 (2007).
26. M. Izaki and T. Omi, *Appl. Phys. Lett.*, **68**, 2439 (1996).
27. Z. H. Gu and T. Z. Fahidy, *J. Electrochem. Soc.*, **146**, 156 (1999).
28. S. Peulon and D. Lincot, *Adv. Mater.*, **8**(2), 166 (1996).
29. J. Elias, R. Tena-Zaera, and C. Lévy-Clément, *Thin Solid Films*, **515**(24), 8553 (2007).
30. Th. Pauporté and D. Lincot, *Journal of Electroanalytical Chemistry*, **517**(1–2), 54 (2001).
31. J. Elias, R. Tena-Zaera, and C. Lévy-Clément, *J. Phys. Chem. C*, **112**(15), 5736 (2008).
32. B. Marí, M. Tortosa, M. Mollar, J. V. Boscà, and H. Cui, *Optical Materials*, **32**(11), 1423 (2010).
33. J. Cembrero, D. Busquets-Mataix, E. Rayón, M. Pascual, M. A. Pérez Puig, and B. Marí, *Materials Science in Semiconductor Processing.*, **16**, 211 (2013).
34. F. Cardon and W. P. Gomes, *Phys. D: Appl. Phys.*, **11**, L63 (1978).
35. C. F. Windisch and G. J Exarhos, *J. Vac. Sc. Technol. A*, **18**, 1677 (2000).
36. I. Mora-Seró, F. Fabregat-Santiago, B. Denier, J. Bisquert, R. Tena-Zaera, J. Elias, and C. Lévy-Clément, *Appl. Phys. Lett.*, **89**, 203117 (2006).
37. Alain P. Roth, James B. Webb, and Digby F. Williams, *Physical Review B*, **25**(12), 7836 (1982).
38. Chang Eun Kim, Pyung Moon, Sungyeon Kim, Jae-Min Myoung, Hyeon Woo Jang, Jungsik Bang, and Ilgu Yun, *Thin Solid Films*, **518**(22), 6304 (2010).
39. W. S. Baer. *Phys. Rev.*, **154**, 785 (1967).
40. N. R. Aghamalyan, E. A. Kafadaryan, R. K. Hovsepyan, and S. I. Petrosyan. *Semicond. Sci. Technol.*, **20**(1), 80 (2005).

Query

Q1: AU: Please provide a digital object identifier (doi) for Ref(s) 20. For additional information on doi's please select this link: http://www.doi.org/. If a doi is not available, no other information is needed from you.